EVS26
Los Angeles, California, May 6 - 9, 2012

Safety Management for Electric Vehicle Batteries in a Tropic Environment

Nora Martiny[1], Patrick Osswald[1], Christian Huber[1], Andreas Jossen[2]
[1] *TUM CREATE Ltd., 62 Nanyang Drive, Blk N1.2, Level 1-28/29, Singapore 637459*
nora.martiny@tum-create.edu.sg
[2] *Technical University of Munich (TUM), Institute for Electrical Energy Storage Technology*

Abstract

To ensure the safety of a battery system certain measures can be employed. Monitoring the actual battery temperature is crucial to guarantee a safe use of the system while an optimized cooling system for the battery pack helps to improve the liability, prevent safety shut-offs and extend the battery's lifetime. Additionally, possibilities to monitor the state of health of the battery on a longer time scale are necessary to avoid over-stretching the battery's capability of storing energy on the one hand and to reduce investment costs on the other hand.
This paper deals with different approaches to handle the battery temperature, especially under challenging tropical outside conditions. A temperature distribution model is developed and evaluated using combined data from a sensor matrix and an infrared camera. This method is used for real-time temperature measurements to investigate and monitor the temperature distribution on pouch cells. The simulation of different cooling systems is presented to show the need of a steady temperature distribution within a battery pack. The goal is to avoid excessive load on certain cells, which has a high impact on a safe use of the pack and reduces lifetime significantly. Finally, an approach to characterize the battery thermodynamically is presented. This is expected to be a useful tool to measure and monitor the state of health of a battery and first investigations are shown for different cell chemistries, performed on commercially available full cells.

Keywords: battery, battery model, cooling, safety, thermal management

1 Introduction

The design of customized energy storage systems for electric vehicles (EVs) is a well-known problem. A highly limited driving range combined with high monetary costs, heavy weight and a time-consuming charging are only some of the challenges that need to be faced within the next years of battery research. In the last couple of months news about battery fire in vehicles or already during shipment have raised the attention to an even more critical topic: battery safety. A recent study issued by the U.S. Department of Transportation Federal Aviation Administration names an average of about 27 % of accidents attributable to lithium battery fire out of all cargo airplane accidents predicted between 2011 and 2020 [1]. The Chevrolet Volt caught fire three weeks after a routine crash test which might have been caused by a coolant leak [2]. Among others, the previously mentioned incidents demand different actions in the field of battery safety from researchers.

The TUM CREATE Centre for Electromobility, Singapore, a joint research program

between Technical University of Munich (TUM), Germany, and Nanyang Technological University (NTU), Singapore, founded by the Singaporean National Research Foundation (NRF), is dealing with all aspects of electromobility in an urban, tropic environment. The research ranges from fundamental investigations on new materials for batteries over vehicle development up to infrastructure and mobility concepts.
Talking about battery safety, the tropic environment in Singapore with all-year average temperatures between 25 °C and 31 °C [3] makes temperature monitoring and active cooling systems even more crucial than for areas with moderate climate conditions. High temperatures deplete battery lifetime significantly and bear the risk of over-heating and, in the worst case, a thermal runaway of the cell [4]. Reliable active cooling systems for the EV's battery pack as well as permanent temperature monitoring are therefore required. The latter helps to recognize safety lacks in the cells at an early stage if active cooling systems fail or are not available.

Another important aspect concerning safety is the state of health (SOH) of the battery cells. Typically, the internal resistance increases with the battery age, resulting in a higher heat generation. This characteristic has to be taken into account for dimensioning the battery management system properly. High currents and high temperatures during operation as well as inaccurate charging algorithms can lead to internal short-circuits in the cells and can cause faster aging or a thermal runaway in the worst case. This makes SOH determination a crucial safety aspect. The author's approach is to use data gained from temperature and open circuit voltage monitoring to determine the SOH of the single cells within a battery pack.

The remainder of this paper is organized as follows: In section 2 the used cell is described and monitoring techniques together with a 2-dimensional approximation for the temperature distribution on the selected cell are presented. Section 3 evaluates and compares different active cooling systems for an EV's battery pack, while section 4 introduces thermodynamic measurement on batteries which is considered to be a valuable tool for battery state determination. The authors finally conclude the paper in section 5 and give a short outlook on next steps.

2 Temperature Measurement

In order to gain information on temperature distribution and thermal behavior of Li-Ion cells, temperature monitoring needs to be applied. Temperature sensors are therefore attached to the cell surface and provide temperature data under laboratory conditions as well as during operation in an EV. While for a detailed analysis of the cells it is necessary to cover as many space of the cell as possible with sensors, for operational applications the amount needs to be reduced due to power consumption, a high effort of data processing and high monetary costs. Nevertheless, it is important to have broad information on the temperature distribution of the whole cell to adapt active cooling systems respectively and minimize damages and aging in the cell. Data from a sensor matrix that has been attached to the cell surface for detailed analysis are therefore compared with infrared (IR) data in order to gain a significant temperature distribution model for normal cell operation.

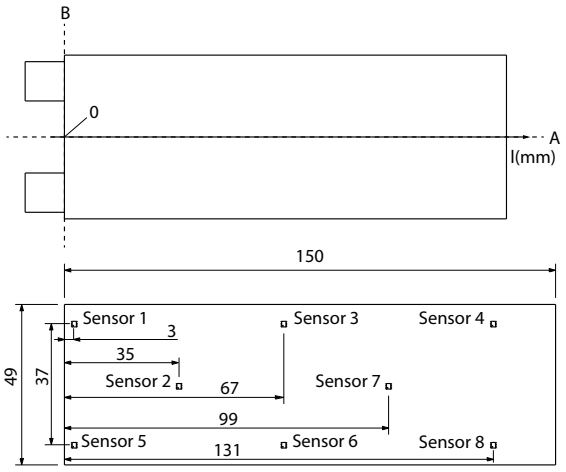

Fig. 1: Sketch of the used pouch cell (above) and temperature sensor board with sensor distribution, numbering and dimensions in mm (below). The terminals of the cell are visible at the left side.

2.1 Cell Description

For first investigations of the applied methods, the authors are using a 5800 mAh high performance Li-ion pouch bag cell from *SLS APL*. With dimensions of 50 mm × 135 mm × 10 mm (W x L x H), an operating temperature range of −10 °C to 50 °C, a discharge current up to 174.0 A, a nominal voltage of 3.7 V, and an energy density of 150 Wh/kg, the cell is suitable for light EV applications.

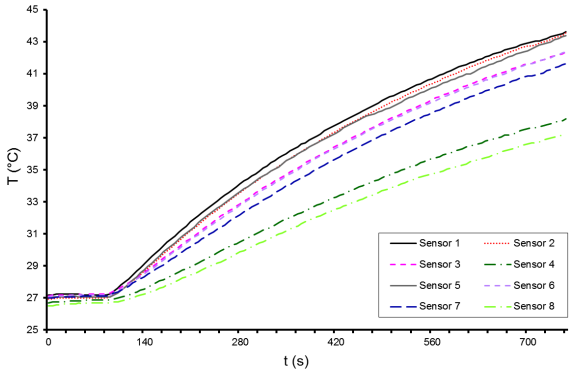

Fig. 2: Dynamic temperature distribution measured with a matrix of eight TMP112 sensors during a 12C-5s pulse charging/discharging cycle

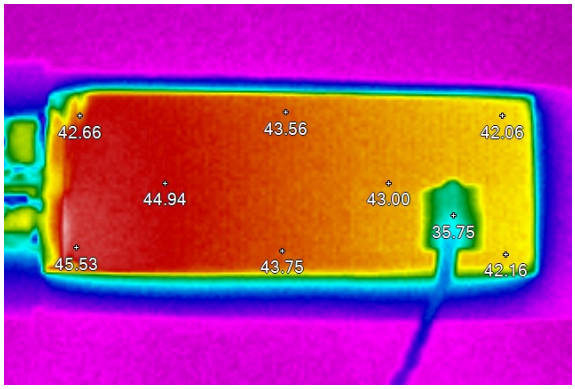

Fig. 3: Temperature distribution measured with an IR camera along axis A (see Fig. 1) after 10 min of a 12C-5s pulse charging/discharging cycle

2.2 Temperature Sensing

In the first step a matrix of eight temperature sensors is applied to the surface of the above described cell. As sensors *TMP112* digital temperature sensor from *Texas Instruments* are used. The sensors are well feasible for battery applications due to their low current consumption, a wide power supply range, small size and a temperature measurement range that covers the operating temperature range of the battery cell very well (−40 °C to 125 °C). The sensor matrix has been placed on a board with the dimensions 50 mm × 150 mm (W x L). The dimensions of board and cell as well as the sensor distribution on the board can be seen in Fig. 1. The terminals of the cell are visible on the left side of the cell. From the sensors data are transmitted via an I2C bus to a micro-controller and therefrom processed to a PC via USB. The data analysis is performed by a MATLAB script.
Fig. 2 shows the dynamic temperature distribution measured by all eight sensors during a 12C pulse charging and discharging cycle. The sensors have first been acclimatized at 27 °C for 2 min. After that, the cell has been charged and discharged with pulses of 5 s duration at 12C for 10 min. It shows that the measured values on all sensors where approximately the same at the beginning of the cycling. After 10 min the measured temperature difference between the terminals and the opposite site of the cell is already more than 5.5 K. Differences between sensors along all axes parallel to axis B are in the range of the specified measuring inaccuracy of the sensors of 0.5 K and can therewith be neglected.

2.3 Infrared Imaging

In order to gain information on the temperature distribution between the sensors as well and for verification of the measured values, images have been taken with an infrared camera at the beginning and at the end of the test cycle. Fig. 3 shows the static temperature distribution after the 10 min pulse charging and discharging test cycle with the terminals at the left side. At the right lower corner of the picture a temperature sensor that is required for safety monitoring from the *BaSyTec* battery tester can be seen. Due to the good heat conducting properties of the sensing cable combined with a poor thermal interface between the sensor and the cell, the temperature at the sensor is significantly lower than the cell temperature.

The temperature distribution evaluation along axis A and its parallel translations through the sensor positions is demonstrated in Fig. 4. Although the influencing temperature sensor from the battery tester can be seen in the diagram as well (green encircled area), due to the big temperature difference of over 7 K compared to its surrounding it can be easily deducted. The diagram shows furthermore, that in areas where the battery tester's sensor is not attached (level of sensors 1, 3, 4) the quasi-linear characteristic of the temperature distribution is pursued. The presented data have been filtered with a simple order-5 moving average FIR filter to eliminate noise that is caused by the inaccuracy of the infrared camera. The filter equation is given in eq. (1) as follows:

$$T_{p,filtered} = \frac{\sum_{i=p-2}^{p+2} T_i}{5} \qquad (1)$$

with T_p as the temperature at a position p on axis A, having p as the distance in pixel from the terminals on the IR picture.

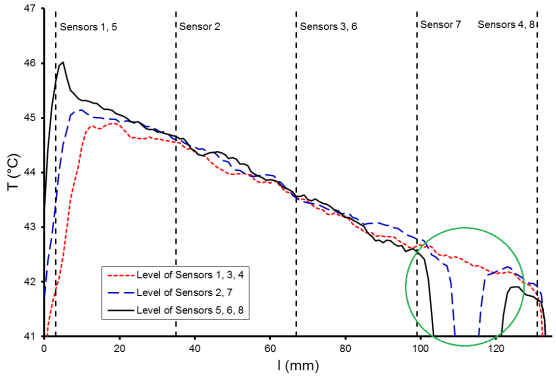

Fig. 4: Temperature distribution measured with an IR camera along axis A (see Fig. 1) after 10 min of a 12C-5s pulse charging/discharging cycle, filtered with an order-5 moving average filter. The green circle shows the area where the temperature sensor of the battery tester influenced the IR image (see Fig. 3)

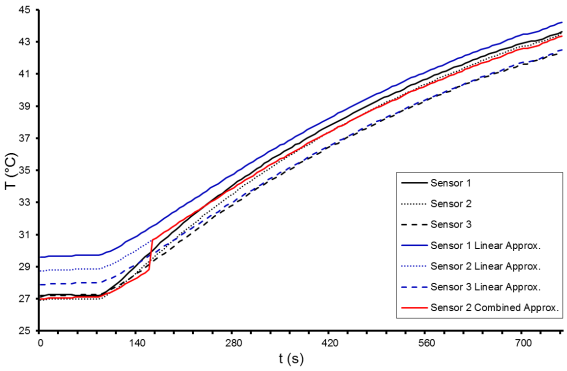

Fig. 5: Comparison of linear approximated data and measured sensor data

2.4 Temperature Distribution Model

For the development of a first temperature distribution model, static temperature data after a 10 min pulse charging and discharging cycle have been collected as described above (see also Fig. 4). After that, the model is applied to dynamic temperature data for evaluation.

2.4.1 Static Temperature Distribution Model

The static temperature distribution along axis A can be approximated by a linear equation

$$T = \alpha l + T_{measured} - \alpha * l_{measured} \qquad (2)$$

where T [°C] is the temperature at a point l. $T_{measured}$ represents the measured temperature at a defined point $l_{measured}$ on axis A, having l as the distance in mm from the terminals . The temperature gradient over the distance l can be approximated with $\alpha = -0.027\,\frac{°C}{mm}$. Comparing the values gained from this equation with the measured values leads to a discrepancy of less than 0.4 K (less than 1 %). This is within the tolerance of the sensor which is defined as ±0.5 K.
Looking at the distribution along axis B (see Fig. 1) the values can be assumed as fixed. For any point on this axis the temperature difference between any other point on the axis is less than 0.2 K (less than 0.5 %) which is within the sensor's tolerance. This assumption is valid for all parallel translations of axis B.

Taking the above mentioned findings into account makes it possible to build a 2-dimensional model of the static surface temperature distribution of the mentioned cell by placing only one temperature sensor on the surface.
The positioning of the sensor is depending on the desired application and accuracy of the model. If the measured temperature is meant to give only a rough estimation of the cell temperature condition and to prevent the cell from overheating, placing the sensor on axis A (see Fig. 1) next to the terminals, where the temperature is highest (compare Fig. 3 and Fig. 4) is considered best. As the temperature distribution in the cell is quasi-linear, for a more precise model that approximates the temperature distribution in the whole cell, the sensor is best positioned in the middle of the cell in order to minimize the error in both directions along axis A.

2.4.2 Dynamic Temperature Distribution Model

For validation of the linear approach and evaluation of the model for dynamic temperature distributions data from Sensor 7 on the sensing board have been taken to calculate the values at the positions of the other sensors by using eq. (2). Fig. 5 shows the comparison for sensors 1, 2 and 3.
While in the passive state of the battery the approximation differs from the measured values by about 2.5 K, the measurement curve and the approximated curve match well after a maximum time of 3 min from the beginning of the pulse cycling for Sensor 1 next to the terminals. The error is less than 0.5 K. For the other measurement points the difference of less than 0.5 K is achieved within a maximum time of 1 min after the beginning of the pulse cycling.
For getting a more precise approximation also for the passive state of the battery cell, a second sensor can be placed next to the terminals. If the measured temperatures at both

sensors are the same, the passive state is assumed. Therewith, the temperature on the whole cell surface can be approximated as equal. In contrast, the active state applies if the temperatures measured on both sensors defer by more than 0.5 K and therewith eq. (2) is valid. In Fig. 5 the red dotted line represents this approach for Sensor 2.
Although the combined approximation is a better approach for modeling the temperature distribution with a minimized error, the second sensor is not mandatory for safety monitoring. The linear approximation provides always temperature values that are higher or equal to the values that have been measured by the sensor matrix. Hence, the linear approach for modeling the temperature distribution or the one-sensor approach without distribution modeling are both sufficient if only overheating needs to be avoided.
For future applications the described normal-operation temperature distribution model can serve as a reference to detect discrepancies in real applications that can be an early indicator for safety relevant failures. However, the sensor matrix used for this publication needs to be optimized as for power consumption, monetary costs and size to make it suitable for operation.

3 System cooling topology

The need for uniform temperature distribution within the battery pack brings along the demand for an overall-cooling system. For an appropriate construction two heat transfer problems have to be taken into account. Dissipated heat from the cell needs to be transfered to the coolant by convection. Within a cooling circuit, the dissipated heat is transmitted from the cells to a location where the coolant needs to be replaced or re-cooled. As the tropical environment is characterized by ambient temperatures that lie close to or above operating temperatures, the battery-system needs to be linked to the central vehicle cooling unit which already serves the cabin A/C. This second heat transfer problem is already adressed in the field of conventional automotive engineering. Therefore in the following, the focus lies on the first mentioned problem within the battery pack.
For a compact and lightweight battery pack structure and a reliable heat dissipation, the interface between cells and coolant has to be designed very carefully. Therefore, the impact of different basic interface designs on cooling efficiency will be evaluated in the following section.
In order to numerically simulate and evaluate the efficiency of different setups, basic assumptions concerning the heat dissipation and temperature distribution of single cells have been made. For the following investigations it is assumed that thermal properties of the cell like heat conductivity and heat capacity are isotropic and uniform all across the cell. Approximated thermal material properties have been taken from [5] and [6] and are listed in Table 1.

Table 1: Simplified thermal properties of cell

Heat capacity $[\frac{\mathrm{J}}{\mathrm{kg\,K}}]$	1,010.0
Thermal conductivity $[\frac{\mathrm{W}}{\mathrm{m\,K}}]$	3.0
Thermal contact resistance $[\frac{\mathrm{m^2\,K}}{\mathrm{W}}]$	0.0001

The designed CAD-model reflects the actual dimensions and the basic geometric characteristics of the cell already known from section 2. In the following, a module consisting of 12 single cells shall be investigated. The average volumetric rate of heat generation for each cell has been calculated from experimental data to be approximately $37\,\mathrm{kW/m^3}$ during a 4C discharge. Those data has been collected by comparing the energy amount transfered while charging and discharging and assuming that the noticeable difference is completely dissipated in form of heat. As current density and therefore the generated heat is highest near the terminals and lowest at the remote parts of the cell, a linear one-dimensional distribution between $46\,\mathrm{kW/m^3}$ and $28\,\mathrm{kW/m^3}$ has been assumed resulting in the calculated overall average rate.
Further simplifications include the assumption of adiabatic borders around the module and a fixed thermal contact resistance between cells and cooling structure.
The numerical thermal module mock-up is used to evaluate different interface setups. Fundamental design parameters include area, geometry and material of the interface, coolant material properties and flow variables. Four selected approaches are modeled in ANSYS CFX and presented below. Simulation is carried out steady state with calculation grids consisting of approximately 1 million nodes. To ensure the comparability of the results, all models are designed to keep the cells within the optimum operational temperature range between 30 °C and 35 °C under constant load. All solid components besides the cells are defined to be made of aluminum.

3.1 Simple aircooling

The most obvious way to cool the battery module is to use the given structural casing elements as heat transfer areas and bypass a stream of chilled ambient air. Convective heat transfer can be supported by enlarging the transfer area by attaching cooling pins (Fig. 6). Advantages of the solution lie within the low complexity, the integral design and low manufacturing costs. Although, the space needed for airflow, additional components as blowers etc. and the noisy high

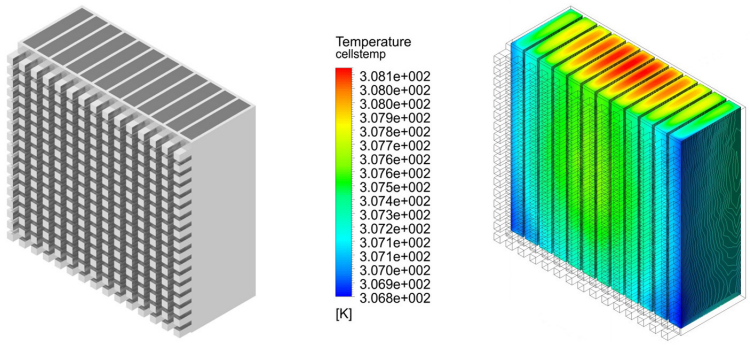

Fig. 6: Temperature distribution within air cooled battery module

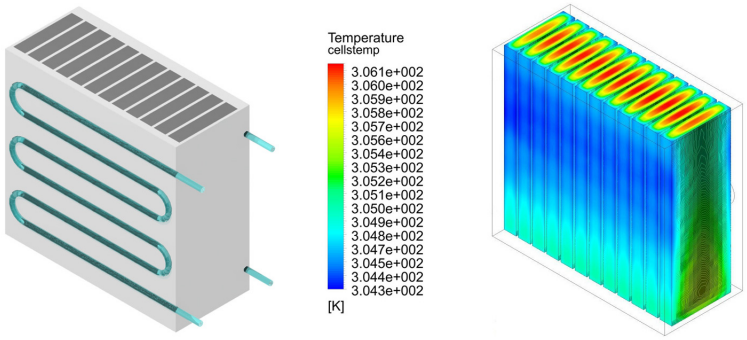

Fig. 7: Temperature distribution within the module cooled by twosided cool plates

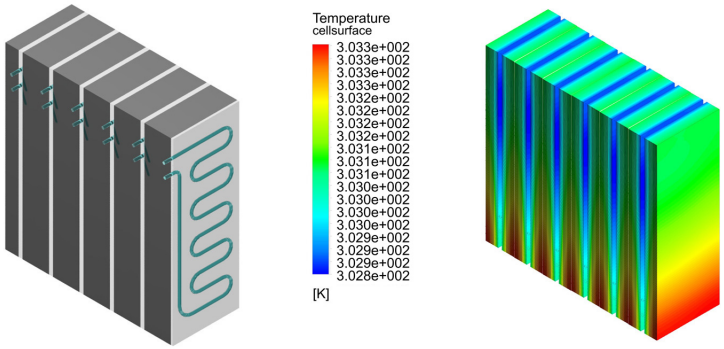

Fig. 8: Temperature distribution within the module with inter-cell fins

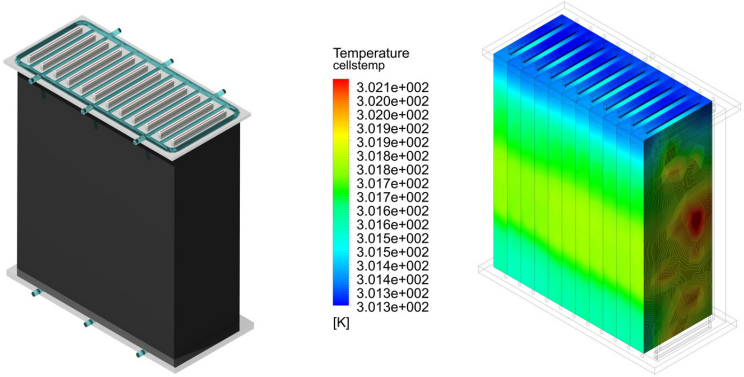

Fig. 9: Temperature distribution within the module cooled via terminals

Table 2: Results of CFD simulation

	Aircooled	Head cooled	Liquid fins	Conductor cooled
Coolant	Air	Water-glycol	Water-glycol	Water-glycol
Coolant T [K]	283	300	300	290
Coolant density [$\frac{kg}{m^3}$]	1.247	1044	1044	1044
Coolant mass flow per cell [$\frac{g}{s}$]	1.65	1.03	0.78	1.12
T max [K]	308.1	306.1	303.3	302.1
T min [K]	306.8	304.3	302.8	301.3
Delta T [K]	1.3	1.8	0.7	0.8
Cooling structure weight [g]	926	1,175	306	742
Cooling structure volume [cm^3]	342	433	110	267

mass-flow rate are disadvantages of a solely air cooled model.

3.2 Liquid cooled head end cooling plates

At some extent, heat transfer from the cell is strictly limited by the coolant's heat capacity. As liquid coolants feature a heat capacity that is higher than that of air by orders of magnitude it is advisable to use them as coolant instead. Therefore, a 50:50 water glycol mix is used for the following three liquid cooled setups. The first one is realized by attaching liquid cooled plates at the cells' lateral edges (Fig. 7).

As expected this setup leads to a high heat-flux at the contact planes and creates a considerable temperature gradient towards the cells' center. Due to the large area cool plates, it reflects the heaviest and bulkiest of all presented solutions.

3.3 Liquid cooled interface fins

In order to achieve a more uniform temperature distribution within the module, coolant channels can be distributed equally spaced between the single cells as shown in Fig. 8. While this technique in fact enables an even temperature distribution, it also comes along with significantly increased system weight, higher manufacturing costs and a complex system setup. Nevertheless, similar systems are already used in commercial vehicles as the Chevrolet Volt [7].

3.4 Liquid cooled conductor cooling

Another approach of cooling the module is to use the metal terminals to thermally connect cells and coolant. For this setup, the terminals were modeled as thin metal plates within the cell, being connected on its both opposite sides. As the terminals' high electric conductivity goes along with a high thermal conductivity, heat can be uniformly dissipated from the cell without the need of an additional structure. However, the crucial design challenge of this setup lies in thermally connecting coolant and electrical system while ensuring a safe electrical isolation at the same time. This can be achieved by applying dielectric ceramics or thermo-silicone on the terminals as shown in Fig. 9. Unfortunately, this interface represents the bottleneck of this approach as thermal conductivity of the dielectric material is significantly below the rest of the system setup. Additionally, the contact area is limited which makes a higher difference in temperature between coolant and cell necessary.

3.5 Evaluation of simulation results

Table 2 gives an overview of the resulting temperature distribution within the cells and the cooling efficiency of the different setups. Besides the thermal characteristics, weight and volume of cooling structure play an important role as well as the overall coolant mass flow per cell.

As seen from the acquired simulation data, the type of cell-coolant interface can have significant influence on the needed cooling power. Therefore, it affects the overall efficiency of EVs especially when used in high-temperature regions. In those regions, a reliable cooling system is not only needed to increase the efficiency but also is a very important safety aspect. Table 2 points out that, if the complexity can be handled, the insertition of liquid cooled foms between the cells offers the lightest and most compact solution. Another approach that seems very promising is the joint use of the terminals for terminal interface as it combines uniform temperature distribution with a compact and simple design that can simultaneously act as structural stabilization element of the module. Given the fact that there is only little public documentation on this setup, its pro-

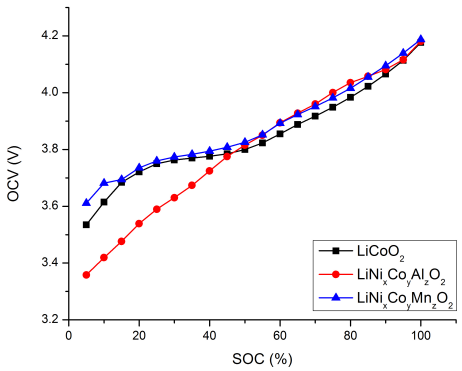

Fig. 10: Dependency of the OCV from the SOC for different $LiMO_2$ cells

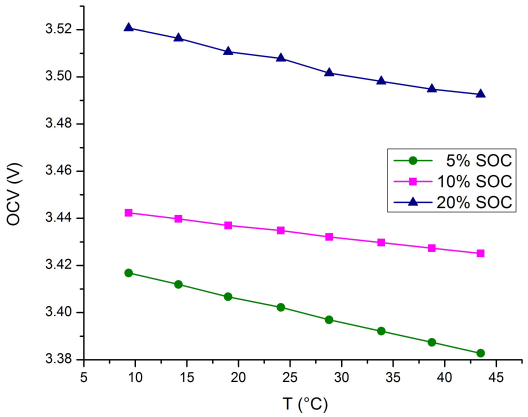

Fig. 11: Dependency of the OCV from the temperature for a $LiCoO_2$ full cell at different SOC

perties and in detail-design should be further investigated by additional tests and physical prototypes.

4 Thermodynamic measurements

As shown in section 2, temperature sensing during operation is a very important task to guarantee user's safety. While thermal management improves safety during the active use, another aspect of research within TUM CREATE focuses on the determination of batteries' state of health (SOH) as an important measure for overlooking actual battery safety conditions. Thermodynamic measurements on batteries are an approach that addresses the long term behavior and reliability of batteries.

Due to the fast growing variety of new anodes, e.g. nano-structured silicon, as well as new cathode composites like $LiMO_2$ (M = Mn, Co, Ni, Al), reliable possibilities for state of health (SOH) and state of charge (SOC) determination have to be developed. Thermodynamic measurements seem to be promising candidates since small changes within the battery structure caused by aging or misuse are believed to have a considerable impact on the calculated profile [8]. Previous research shows that for $LiCoO_2$ half cells [11] as well as for self-made coin cells with different chemistries [9].

The profiles have a valuable fingerprint characteristic and behave additive, i.e., profiles for full cells are weighted sums of the respected half-cell profiles [9].

For an ideal reversible cell, the Gibbs free energy change $\Delta_r G$ can be express by

$$\Delta_r G = -nFE_{emf} \tag{3}$$

with E_{emf} as the electromotive force, which can be assumed to be equivalent to the open circuit voltage of the battery at equilibrium and n as the number of exchanged electrons. The authors assume E_{emf} to be constant for an incremental change δx. The thermodynamic relation between $\Delta_r G$ and the change of entropy ΔS can be expressed as

$$\Delta_r S = \frac{\partial \Delta_r G}{\partial T} \tag{4}$$

Measuring the open circuit voltage at different temperatures allows the calculation of the differential charge/discharge entropy according to

$$\Delta_r S = nF\frac{\partial (OCV(x))}{\partial T} \tag{5}$$

where F is the Faraday constant, $OCV(x)$ the open circuit voltage of the battery in equilibrium at different states of lithiation x in the anode and T is the temperature of the battery. Hence, the value of ΔS describes the change of entropy that occurs when a certain amount of δx lithium is intercalated into the anode during charging. At the same time, the same amount of δx lithium is deintercalated from the cathode. For discharging, δx lithium is deintercalated from the anode and intercalated into the anode. As it can be seen from eq. (5), the entropy change ΔS is positive if the $OCV(x)$ decreases for a certain value of x with increasing temperature.

The OCV for $LiMO_2$ based batteries depends on the state of charge as well as on the temperature of the battery [10]. Fig. 10 shows the occurring change of the OCV fitted on the battery's SOC for different cell chemistries which are commercially available. While $LiNi_xCo_yAl_zO_2$ shows a linear behavior for the full range, $LiCoO_2$ and $LiNi_xCo_yMn_z$ show a small plateau between

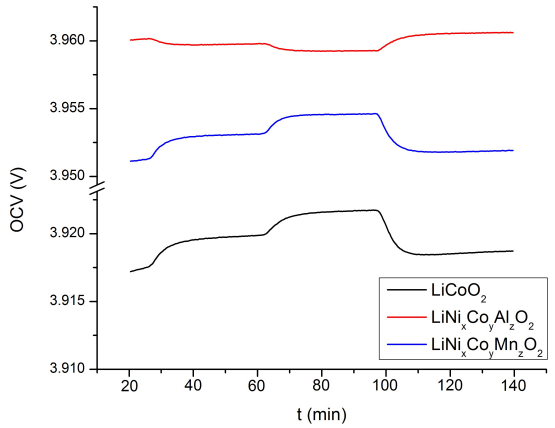

Fig. 12: OCV relaxation for $LiNi_xCo_yAl_zO_2$, $LiCoO_2$ and $LiNi_xCo_yMn_z$ cells after temperature changes of 10 °C for a SOC of 70%

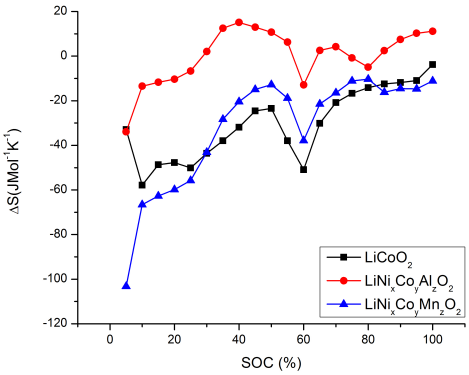

Fig. 13: Calculated entropy profiles from $LiNi_xCo_yAl_zO_2$, $LiCoO_2$ and $LiNi_xCo_yMn_z$ cells

40 % and 20 % SOC before decreasing again linearly. Fig. 11 shows the OCV's dependency on the temperature at three different states of charge for a $LiCoO_2$ battery. The OCV's behavior is also linear for this $LiCoO_2$ cell and is decreasing for higher temperatures. For higher temperatures, the OCV does not reach a stable equilibrium due to the increasing self-discharge of the battery, resulting in inaccurate measurements.

4.1 Experiments

To measure the battery's OCV as well as the temperature, an *Agilent 34972A* with a 20 channel multiplexer is used for achieving the necessary resolution to measure the change of the OCV. The batteries are cycled in an *Espec* climate chamber to control the temperature between 5 °C and 25 °C in steps of 10 °C. The cycling is performed by a *BaSyTec* battery tester. After evaluating the capacity of each cell at a discharge rate of 0.2 C at 25 °C as recommended by the manufacturer, the cell is fully charged using the constant current-constant voltage (CCCV) method. A 0.2 C rate and a constant voltage of 4.2 V respectively is applied. Finally, the cells are discharged with constant steps at a 0.2 C rate for 15 mins each.
After each discharging step, the OCV relaxation is measured for 45 mins. The voltage and temperature measurement interval is chosen to be 30 s. After this, the temperature is decreased by 10 °C down to 15 °C and the OCV behavior is monitored for 45 mins. In the next step, the temperature is decreased for a second time down to 5 °C and the OCV is measured for another 45 mins. Finally, the cell is heated up to 25 °C. To allow the batteries to reach an equilibrium state at 25 °C, the waiting time is 60 mins before the next discharging step is applied.
The necessary data for the calculation of the entropy profile can be gained by performing these measurements until the battery is fully discharged. The *discharged state* is defined when the amount of mAh taken out of the cell reaches the defined discharge capacity. This is done by the coulomb counting method and measured with the *BaSyTec* battery cycler. The second criterion for recognizing the *discharged state* is if the cell voltage drops below 3.0 V, whichever of the criteria comes first. The measurement time can be varied by changing the relaxation time and focusing on certain SOC of interest. Since the measurement time was only five days and the fact that mainly low temperatures were used, the self-discharge of the battery is neglected.

4.2 Results

Fig. 12 shows an example of the OCV relaxation for three different cell chemistries at a state of charge of 70%. For an SOC over 60% as well as a temperature of 25 °C, the time for the OCV relaxation is assumed to be enough to achieve a voltage which can be defined as equilibrium. For lower states of charge and lower temperatures, the measured time of 45 mins seems to be insufficient to reach an OCV which can be assumed to be in an equilibrium state. The relaxation curves where fitted using *Origin* software to estimate the final value of the OCV. These estimations are in good agreement on OCV relaxation tests performed before. The change of entropy from 5% to 0% cannot be determined precisely due to the different possible criteria for the *discharged state* even though the two previously mentioned definitions were in close accordance thanks to the calibration of the cell capacity before every discharge cycle. The OCV for the $LiCoO_2$ and $LiNi_xMn_yCo_zO_2$ based cells increase for lower temperatures for the whole range of SOC. For $LiNi_xCo_yAl_zO_2$ the OCV decreases for lower temperatures only at a SOC of

80%, 60% and smaller than 25% respectively. Therefore, the entropy profile for this cell shows certain areas where the change of entropy ΔS is > 0.
Fig. 13 shows the calculated entropy profiles for different types of cells. These measurements show, that it is possible to upscale previous measurements to larger cells. Therefore, calculated entropy profiles are a possible way of characterizing different cell chemistries and different cell sizes, either for self-made coin cells or commercial 18650 cells. As discussed, changes in the entropy profile help to estimate the battery's temperature excursion during charge and discharge [9] and enable the development of a tool for SOH prediction of a battery [11].

5 Conclusion & Outlook

Operation in tropic environment brings along special safety relevant challanges in battery pack design of which three are presented in this paper. An approach for a monitoring technique has been given and an approximation of 2D temperature distribution has been derived from an experimental sensor setup. The obtained data wer used as input for numerical thermal models of different cell/coolant interfaces. CFD analysis has uncovered significant differences in their efficency and supports the selection of a reliable and compact system.
As long term operational safety strongly depends on the batteries' state of health, its interaction with thermodynamic cell properties has been analysed in detail. Therefore, several test series have been conducted to determine the OCV dependency on temperature for different cell types at variant SOC levels. Based on these results entropy profiles have been calculated.
In order to validate the temperature distribution model, the predicted thermal interface properties and the coherence of module's thermal behaviour and cells' state of health, further tests and physical prototypes are required and will be part of future research within TUM CREATE. Particular attention should be paid to investigations concerning the models' validity for different cell types, chemistry and geometries. Additional findings are likely to be gained by developing advanced sensor techniques and a refined specific numerical simulation model.

Disclaimer

This publication is made possible by the *Singapore National Research Foundation* (NRF) under its CREATE programme. The views expressed herein are solely the responsibility of the authors and do not necessarily represent the official views of the Foundation.

References

[1] United States of America. U.S. Department of Transportation Federal Aviation Administration, *Freighter Airplane Cargo Fire Risk Model*, Washington: U.S. Department of Transportation Federal Aviation Administration, 2011.

[2] *Chevrolet Volt Fire Solution Expected Soon, Coolant Leak May Be The Culprit*, http://www.autoguide.com/autonews/2011/12/chevrolet-volt-fire-solution-expected-soon-coolant-leak-may-be-the-culprit.html, accessed on 2012-01-20.

[3] *Weather and Climate in Singapore*, Internet: http://www.guidemesingapore.com/relocation/introduction/climate-in-singapore, accessed on 2012-01-20.

[4] A. Jossen and W. Weydanz, *Moderne Akkumulatoren richtig einsetzen*, ISBN 3-939359-11-4, Untermeitingen, Inge Reichardt Verlag, 2006.

[5] A. Pesaran and M. Keyser, *Thermal Characteristics of Selected EV and HEV Batteries*, Proceedings of the Annual Battery Conference: Advances and Applications, ISBN 0-7803-6545-3, Long Beach, 2001.

[6] R. Sabbah, R. Kizilel et al, *Active vs. passive thermal management of high power lithium-ion packs: Limitations of temperature rise and uniformity of temperature distribution*, Journal of Power Sources, ISSN 0378-7753, 182(2008), 630-638.

[7] K. Buchholz, *Dana helps cool Volt's battery*, SAE Vehicle Elictrification Magazine 4(2011).

[8] Y. Reynier, R. Yazami and B. Fultz, *The entropy and enthalpy of lithium intercalation into graphite*, Journal of Power Sources, ISSN 0378-7753, 119-121(2003), 850-855.

[9] V. V. Viswanathan et al. *Effect of entropy change of lithium intercalation in cathodes and anodes on Li-ion battery thermal management*, Journal of Power Sources, ISSN 0378-7753, 195(2010), 3720-3729.

[10] K. Takano et al. *Entropy change in lithium ion cells on charge and discharge*, Journal of Applied Electrochemistry, ISSN 0021-8913, 32(2002), 251-258.

[11] Y. Reynier et al. *Entropy of Li intercalation in LixCoO2*, Physical Review B, ISSN 1098-0121, 70(2004).

Authors

Nora Martiny graduated in 2010 at TUM as electrical engineer. Since 2011 she works with TUM CREATE on energy storage systems. Her research focus lies on sensing possibilities for safety monitoring of Li-Ion cells.

Patrick Osswald received his final degree in electrical engineering from TUM in 2010. Since 2011 he is working for TUM CREATE, focusing on battery state determination by using a thermodynamic approach.

Christian Huber completed his studies of aerospace engineering and business administration at TUM in 2011. Within TUM CREATE he now focuses on thermal management of battery packs and thermofluid dynamic simulation.

Andreas Jossen earned his doctorate, dealing with "Management of photo-voltaic plants using energy storage systems" at University of Stuttgart. From 1994 he was group leader for different battery related topics with ZSW, Ulm. Since 2010 he is full professor at the Institute for Electrical Energy Storage Technology, TUM.